Non-intrusive proper generalized decomposition involving space and parameters: application to the mechanical modeling of 3D woven fabrics

Angel Leon[1], Sebastien Mueller[1], Patrick de Luca[1], Rajab Said[1], Jean-Louis Duval[1] and Francisco Chinesta[2*]

*Correspondence:
Francisco.CHINESTA@ensam.eu
[2] ESI Group chair @ PIMM, Arts et Metiers Institute of Technology, 151 Boulevard de l'Hopital, 75013 Paris, France
Full list of author information is available at the end of the article

Abstract

In our former works we proposed different Model Order Reduction strategies for alleviating the complexity of computational simulations. In fact we proved that separated representations are specially appealing for addressing many issues, in particular, the treatment of 3D models defined in degenerated domains (those involving very different characteristic dimensions, like beams, plate and shells) as well as the solution of parametrized models for calculating their parametric solutions. However it was proved that the efficiency of solvers based on the construction of such separated representations strongly depends on the affine decompositions (separability) of operators, parameters and geometry. Even if our works proved that different techniques exists for performing such beneficial separation prior of applying the separated representation constructor, the complexity of the solver increases in certain circumstances too much, as the one involving the space separation of complex microstructures concerned by 3D woven fabrics. In this paper we explore an alternative route that allows circumventing the just referred difficulties. Thus, instead of following the standard procedure that consists of introducing the separated representation of the unknown field prior to discretize the models, the strategy here proposed consists of proceeding inversely: first the model is discretized and then the separated representation of the discrete unknown field is enforced. Such a procedure enables the consideration of very complex and non separable features, like complex domains, boundary conditions and microstructures as the ones concerned by homogenized models of complex and rich 3D woven fabrics. It will be proved that such a procedure can be also easily coupled with a non-intrusive treatment of the parametric dimensions by using a sparse hierarchical collocation technique.

Keywords: Model Order Reduction, In-plane-out-of-plane separated representations, Parametric solutions, Non-intrusice PGD

Introduction

A lot of models in polymer, metals and composites processing, structural mechanics, among many others, are defined in degenerated three-dimensional domains. By degenerated we understand that at least one of the domain characteristic dimensions is much

smaller than the others, as usually encountered when addressing plate and shells geometries.

Mesh-based solutions of 3D models defined in such degenerated domains remain even nowadays a recurrent issue because the resulting meshes usually involve too many degrees of freedom. In that case the first question concerns the possibility of reducing the model complexity. In the past many simplified (1D or 2D) models were derived by introducing simplifying hypotheses into the general 3D problem, however in many cases the required hypotheses fail and such a reduction is not possible anymore. In those circumstances only fully 3D solutions are conceivable with the difficulty associated to the extremely large discrete linear systems resulting from employed meshes that must be fine enough for attaining the expected accuracy.

Thus, from one side 3D solutions seem mandatory in many cases, but on the other side, such solutions remain computationally challenging for most of mesh-based discretization techniques. Thus, new approaches able to address the efficient solution of such models are required.

Space separated representations within PGD—Proper Generalized Decomposition—framework seems a valuable route for alleviating such difficulties as discussed below. The interested reader can refer to the abundant references on the PGD, among them [1–4] and the references therein. Multi-resolution features of separated representations were addressed in [5].

Sometimes the spatial domain Ξ, assumed three-dimensional, can be separated using an in-plane-out-of-plane separated representation specially appropriate for addressing problems defined in plate or shell-like geometries. In that case the domain Ξ can be expressed as $\Xi = \Omega \times \mathcal{I}$, with $\Omega \subset \mathbb{R}^2$ and $\mathcal{I} \subset \mathbb{R}$.

In-plane-out-of-plane separated representations are particularly useful for addressing the solution of problems defined in plate [6], shell [7] or extruded domains [8]. A parametric 3D elastic solution of beams involved in frame structures was proposed in [9]. The same approach was extensively considered in structural plate and shell models in [10–15]. Space separated representations were enriched with discontinuous functions for representing cracks in [16], delamination in [17] and thermal contact resistances in [18]. Domain decomposition within the separated space representation was accomplished in [19] and localized behaviors were addressed by using superposition techniques in [20].

The in-plane-out-of-plane decomposition was then extended to many other physics: thermal models were considered in [18]; squeeze flows of Newtonian and non Newtonian fluids in laminates in [21]; flows in stratified porous media in [22] an nonlinear viscoplastic flows in plate domains in [23]. A full space decomposition was also efficiently applied for solving the Navier–Stokes equations in the lid-driven cavity problem in [24–26].

In all these works we proved that separated representations are specially appealing for addressing many issues, in particular, the treatment of 3D models defined in degenerated domains (those involving very different characteristic dimensions, like beams, plates and shells) as well as the solution of parametrized models for calculating their parametric solutions. However it was proved that the efficiency of solvers based on the construction of such separated representations strongly depends on the affine decompositions (separability) of operators, parameters and geometry. Even if our works proved that different techniques exists for performing such beneficial separation prior of applying the separated representation constructor, the complexity of the solver increases in certain circumstances too

much, as the one involving the space separation of complex microstructures concerned by 3D woven fabrics.

In this paper we explore an alternative route that allows circumventing the just referred difficulties. Thus, instead of following the standard procedure that consists in introducing the separated representation of the unknown field prior to discretize the models, the strategy here proposed consists of proceeding inversely: first the model is discretized and then the separated representation of the discrete unknown field is enforced. Such a procedure, that we never considered in our former developments, and that constitutes the main contribution of the present work, enables the consideration of very complex and non separable features, like complex domains, boundary conditions and microstructures as the ones concerned by homogenized models of complex and rich 3D woven fabrics. It will be proved that such a procedure can be also easily coupled with a non-intrusive treatment of the parametric dimensions by using a sparse hierarchical collocation technique.

Standard separated representation

The Proper Generalized Decomposition of a generic model defined in a plate domain $\Xi = \Omega \times \mathcal{I}$ with $(x, y) = \mathbf{x} \in \Omega \subset \mathbb{R}^2$ and $z \in \mathcal{I} = [0, H] \subset \mathbb{R}$, and involving the unknown field $u(\mathbf{x}, z)$, consists of looking for the in-plane-out-of-plane separated representation

$$u(\mathbf{x}, z) \approx \sum_{j=1}^{N} X_j(\mathbf{x}) \cdot Z_j(z), \tag{1}$$

that introduced into the problem weak form results in two problems, the first for computing the functions involving the in-plane coordinates ($X_j(\mathbf{x})$) and the other the ones related to the through-the-thickness coordinate ($Z_j(z)$).

For the sake of completeness, we summarize in Appendix , the standard procedure for constructing the solution separated representation (1).

Discussion

The standard procedure described in Appendix is very powerful as widely proved in our former works, and allows for a very compact solution structure, impressive computing time savings and extremely fine resolution along the thickness coordinate that results into a 1D problem that can be solved easily and efficiently independently of the number of nodes considered along the thickness direction, however, many technical difficulties remain, being the most relevant:

- The procedure is very intrusive because it needs a new algorithmic structure, quite different to the standard finite element;
- The assembling of plate domains for constituting a complex structure remains nowadays a tricky issue when operating with such a separated representations;
- When considering nonlinear models the computational complexity increases significantly;
- Most importantly, the success of the just described procedure is based on affine structure of both the differential operators and the model parameters, like the thermal conductivity in the problem considered in Appendix A. In complex microstructures, as the one involved in the 3D woven fabrics depicted in Fig. 1 that will be considered
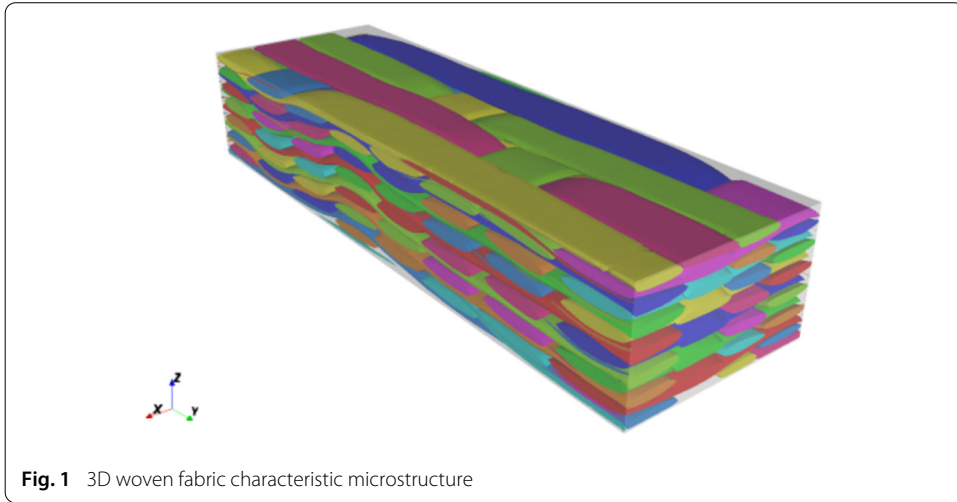
Fig. 1 3D woven fabric characteristic microstructure

later, affine decompositions of material properties are compromised making difficult the use of standard procedures based on the use of separated representations. Even if one could envisage the application of the singular value decomposition—SVD—for obtaining that affine structure, SVDs will involve an extremely large number of terms. Moreover, the application of the SVD has a significant computational cost, magnified when addressing nonlinear behaviors needing for repeated decompositions.

In the next section we propose an alternative procedure that allows circumventing the just referred difficulties. Thus, instead of following the discussed standard procedure that consists in introducing the separated representation of the unknown field prior to discretize the model, the strategy here proposed consists of proceeding inversely: first the model is discretized and then the separated representation of the discrete unknown field is enforced.

Non-intrusive formulation: discretizing first and then enforcing a separated representation

As just indicated, the proposed strategy enforces the unknown field separation on the discrete form accomplished by using any standard well experienced discretization technique. In what follows and without loss of generality we assume a finite element discretization.

Again, for the sake of simplicity we start considering a laminate, and an scalar unknown field, to address more complex configurations later.

Standard 3D finite element discretization

When considering a standard 3D finite element approximation and discretization on a mesh, compatible with the stratified domain structure, the resulting discrete form reads

$$\mathbf{GU} = \mathbf{F}, \tag{2}$$

where vector $\mathbf{U}$ contains the nodal unknowns.

Re-numbering by layering

As just indicated, we assume that the finite elements mesh follows the laminate layers. If along the plate thickness we assume a finite element layer, and denotes by $\mathbf{U}_i, i = 1, \ldots, \mathcal{T}$, the nodal degrees of freedom associated to nodes belonging to the layer $\mathcal{L}_i, i = 1, \ldots, \mathcal{T}$, employing an adequate nodal re-numbering, system (2) can be rewritten as

$$
\begin{pmatrix}
\mathbf{G}_{11} & \mathbf{G}_{12} & \cdots & \mathbf{G}_{1\mathcal{T}} \\
\mathbf{G}_{21} & \mathbf{G}_{22} & \cdots & \mathbf{G}_{2\mathcal{T}} \\
\vdots & \vdots & \ddots & \vdots \\
\mathbf{G}_{\mathcal{T}1} & \mathbf{G}_{\mathcal{T}2} & \cdots & \mathbf{G}_{\mathcal{T}\mathcal{T}}
\end{pmatrix}
\begin{pmatrix}
\mathbf{U}_1 \\
\mathbf{U}_2 \\
\vdots \\
\mathbf{U}_{\mathcal{T}}
\end{pmatrix}
=
\begin{pmatrix}
\mathbf{F}_1 \\
\mathbf{F}_2 \\
\vdots \\
\mathbf{F}_{\mathcal{T}}
\end{pmatrix}.
\tag{3}
$$

Separated expression of the unknown vector

Now, inspired from the in-plane-out-of-plane separated representation employed in "Standard separated representation" section, we assume

$$
\mathbf{U}_i = \mathbf{V} \, W_i,
\tag{4}
$$

where W_i is the i-component of vector $\mathbf{W}$ that scales the evolution of $\mathbf{V}$ along the domain thickness, with $i \in [1, \ldots, \mathcal{T}]$.

Equation (4) can be rewritten as

$$
\mathbf{U}_i = \mathbb{W}_i \mathbf{V}
\tag{5}
$$

with

$$
\mathbb{W}_i =
\begin{pmatrix}
W_i & 0 & \cdots & 0 \\
0 & W_i & \cdots & 0 \\
\vdots & \vdots & \ddots & \vdots \\
0 & 0 & \cdots & W_i
\end{pmatrix}
= W_i
\begin{pmatrix}
1 & 0 & \cdots & 0 \\
0 & 1 & \cdots & 0 \\
\vdots & \vdots & \ddots & \vdots \\
0 & 0 & \cdots & 1
\end{pmatrix}
= W_i \mathbf{I}.
\tag{6}
$$

Using the just introduced notation, the layered nodal unknown vector reads:

$$
\begin{pmatrix}
\mathbf{U}_1 \\
\mathbf{U}_2 \\
\vdots \\
\mathbf{U}_{\mathcal{T}}
\end{pmatrix}
=
\begin{pmatrix}
W_1 \mathbf{I} \\
W_2 \mathbf{I} \\
\vdots \\
W_{\mathcal{T}} \mathbf{I}
\end{pmatrix}
\mathbf{V},
\tag{7}
$$

that can be expressed in the compact form

$$
\mathbf{U} = \mathbb{Z} \mathbf{V}.
\tag{8}
$$

Introducing expression (7) into the linear system (3) it results

$$
\begin{pmatrix}
\mathbf{G}_{11} & \mathbf{G}_{12} & \cdots & \mathbf{G}_{1\mathcal{T}} \\
\mathbf{G}_{21} & \mathbf{G}_{22} & \cdots & \mathbf{G}_{2\mathcal{T}} \\
\vdots & \vdots & \ddots & \vdots \\
\mathbf{G}_{\mathcal{T}1} & \mathbf{G}_{\mathcal{T}2} & \cdots & \mathbf{G}_{\mathcal{T}\mathcal{T}}
\end{pmatrix}
\begin{pmatrix}
W_1 \mathbf{I} \\
W_2 \mathbf{I} \\
\vdots \\
W_{\mathcal{T}} \mathbf{I}
\end{pmatrix}
\mathbf{V}
=
\begin{pmatrix}
\mathbf{F}_1 \\
\mathbf{F}_2 \\
\vdots \\
\mathbf{F}_{\mathcal{T}}
\end{pmatrix},
\tag{9}
$$

that premultiplying by the transpose of $\mathbb{Z}$ we finally obtain a linear system whose size scales with the number of nodes in the plane, that is, in each of the $\mathcal{T}$ layers

$$(W_1\mathbf{I}\ W_2\mathbf{I}\ \cdots\ W_{\mathcal{T}}\mathbf{I}) \begin{pmatrix} \mathbf{G}_{11} & \mathbf{G}_{12} & \cdots & \mathbf{G}_{1\mathcal{T}} \\ \mathbf{G}_{21} & \mathbf{G}_{22} & \cdots & \mathbf{G}_{2\mathcal{T}} \\ \vdots & \vdots & \ddots & \vdots \\ \mathbf{G}_{\mathcal{T}1} & \mathbf{G}_{\mathcal{T}2} & \cdots & \mathbf{G}_{\mathcal{T}\mathcal{T}} \end{pmatrix} \begin{pmatrix} W_1\mathbf{I} \\ W_2\mathbf{I} \\ \vdots \\ W_{\mathcal{T}}\mathbf{I} \end{pmatrix} \mathbf{V}$$

$$= (W_1\mathbf{I}\ W_2\mathbf{I}\ \cdots\ W_{\mathcal{T}}\mathbf{I}) \begin{pmatrix} \mathbf{F}_1 \\ \mathbf{F}_2 \\ \vdots \\ \mathbf{F}_{\mathcal{T}} \end{pmatrix}, \tag{10}$$

whose matrix compact form reads

$$\left[\mathbb{Z}^T\mathbf{G}\mathbb{Z}\right]\mathbf{V} = \mathbb{Z}^T\mathbf{F}, \tag{11}$$

that as soon as matrix $\mathbb{Z}$ is known, from the vector $\mathbf{W}$ involved in the decomposition of $\mathbf{U}$, the reduced matrix $\mathbb{Z}^T\mathbf{G}\mathbb{Z}$ can be computed and the linear system solved for obtaining vector $\mathbf{V}$ whose size is characteristic of a 2D problem.

It is also important to note that this solution only implies matrix products and the solution of a linear system of reduced size, tasks that can be massively parallelized in adequate computing platforms.

Now, as soon as $\mathbf{V}$ is available, we should update vector $\mathbf{W}$. For that purpose the previous systems must be expressed differently as discussed below.

In the present case the unknown vector $\mathbf{U}$ reads

$$\begin{pmatrix} \mathbf{U}_1 \\ \mathbf{U}_2 \\ \vdots \\ \mathbf{U}_{\mathcal{T}} \end{pmatrix} = \begin{pmatrix} \mathbf{V} & \mathbf{0} & \cdots & \mathbf{0} \\ \mathbf{0} & \mathbf{V} & \cdots & \mathbf{0} \\ \vdots & \vdots & \ddots & \vdots \\ \mathbf{0} & \mathbf{0} & \cdots & \mathbf{V} \end{pmatrix} \mathbf{W}, \tag{12}$$

that can be expressed in the compact form as

$$\mathbf{U} = \mathbb{P}\mathbf{W}, \tag{13}$$

that allows reducing the linear system to a size that scales with the number of nodes along the thickness direction

$$\left[\mathbb{P}^T\mathbf{G}\mathbb{P}\right]\mathbf{W} = \mathbb{P}^T\mathbf{F}, \tag{14}$$

that as soon as matrix $\mathbb{P}$ is known, from vector $\mathbf{V}$ involved in the decomposition of $\mathbf{U}$, the reduced matrix $\mathbb{P}^T\mathbf{G}\mathbb{P}$ can be computed and the linear system solved for obtaining vector $\mathbf{W}$ whose size is characteristic of a 1D problem.

We note again that this solution only implies matrix products and the solution of a linear system of reduced size, tasks that can be massively parallelized in adequate computing platforms.

Separated representation constructor

Obviously the solution $\mathbf{U}$ cannot be expressed as a single term involving vectors $\mathbf{V}$ and $\mathbf{W}$. If we assume that N terms are required in the separated representation, i.e. the unknown vector is expressed from one of the two (equivalent) expressions below:

$$\mathbf{U} \approx \sum_{j=1}^{N} \mathbb{Z}^j \mathbf{V}^j, \tag{15}$$

with $\mathbb{Z}^j$ depending on $\mathbf{W}^j$, or

$$\mathbf{U} \approx \sum_{j=1}^{N} \mathbb{P}^j \mathbf{W}^j, \tag{16}$$

with $\mathbb{P}^j$ depending on $\mathbf{V}^j$, and that at the present iteration the first $n-1$ terms were already calculated, i.e.

$$\mathbf{U}^{n-1} = \sum_{j=1}^{n-1} \mathbb{Z}^j \mathbf{V}^j, \tag{17}$$

or

$$\mathbf{U}^{n-1} = \sum_{j=1}^{n-1} \mathbb{P}^j \mathbf{W}^j, \tag{18}$$

now, the calculation of the enriched approximation $\mathbf{U}^n$ requires computing $\mathbf{V}^n$ and $\mathbf{W}^n$.

As discussed in the previous section we must compute $\mathbf{V}^n$ by assuming $\mathbf{W}^n$ known, and then update $\mathbf{W}^n$ from the just calculated $\mathbf{V}^n$. The iteration continues until reaching the fixed point, and then the next couple of vectors $(\mathbf{V}^{n+1}, \mathbf{W}^{n+1})$ will be searched.

When looking for vector $\mathbf{V}^n$ with $\mathbf{W}^n$ assumed known, we consider the reduced linear system:

$$\left[\mathbb{Z}^{n^T} \mathbf{G} \mathbb{Z}^n \right] \mathbf{V}^n = -\mathbb{Z}^{n^T} \mathbf{G} \left[\sum_{j=1}^{n-1} \mathbb{Z}^j \mathbf{V}^j \right] + \mathbb{Z}^{n^T} \mathbf{F}, \tag{19}$$

from which $\mathbf{V}^n$ is calculated, leading to the other reduced linear system

$$\left[\mathbb{P}^{n^T} \mathbf{G} \mathbb{P}^n \right] \mathbf{W}^n = -\mathbb{P}^{n^T} \mathbf{G} \left[\sum_{j=1}^{n-1} \mathbb{P}^j \mathbf{W}^j \right] + \mathbb{P}^{n^T} \mathbf{F}, \tag{20}$$

from which $\mathbf{W}^n$ is updated.

Discussion

The just described procedure deserves the following important comments:

- Matrix $\mathbf{G}$ is obtained with any discretization technique, in particular any finite element software using any type of finite element. In this sense the just described procedure is much less intrusive than the one resulting when introducing the separated representation before its discretization as described in "Standard separated representation"

section (and the associated Appendix). It is important to note that the numerical solutions presented and discussed later, the discretization, that is, the construction of the stiffness matrix $\mathbf{G}$, was accomplished by using the commercial software VPS from ESI Group;

- In the case of nonlinear models matrix $\mathbf{G}$ could correspond to the usual tangent matrix and again it is computed in a standard way, for example finite elements;
- As soon as the matrix $\mathbf{G}$ is available by using any simulation software, the just described procedure can be viewed as an iterative procedure for solving the algebraic system. This iteration strategy can be incorporated as a new function to an existing solver or performed outside. It is in that sense that the procedure is qualified as non-intrusive.
- The proposed strategy could be viewed as an iterative linear solver able to produce a separated representation of the nodal solution;
- When the solution is obtained with the desired accuracy according to Eqs. (15) or (16), it could be post-compressed to reduce, when possible, the number of terms in the finite sum decomposition, from N to $\hat{N}$, with $\hat{N} \leq N$. For that purpose we proceed as described in [4], from which it follows the SVD decomposition of the fully 3D nodal solution (considering as decomposition coordinates the ones related to the plane and thickness);
- The solution procedure only involves matrix products and linear systems solutions (of reduced size, having 2D and 1D complexities) that can be efficiently performed using massively parallel computing architectures;
- The solution procedure can be also viewed as a domain decomposition technique in which continuity conditions are implicitly enforced (during the finite element construction of matrix $\mathbf{G}$) and in which the information spreads all along the whole domain at each iteration.
- Such a strategy is not restricted to in-plane-out-of-plane decompositions, it can be used in any partition of the vector containing the nodal unknowns with the only restriction that all them contains the same number of nodes. It is in that sense that it seems very close to domain decomposition techniques, expressing

$$\mathbf{U} \approx \sum_{i=1}^{\mathcal{D}} \mathbb{D}^j \cdot \mathbf{V}^j, \tag{21}$$

where $\mathbb{D}^j$ depends in vector $\mathbf{D}^j$ of size $\mathcal{D}$, being $\mathcal{D}$ the number of subdomains considered in the partition of $\mathbf{U}$ and with $\mathbf{V}^j$ having the size related to the number of nodes considered in each subdomain. As just claimed vectors $\mathbf{V}^j$ can be associated to nodes located anywhere, even with no direct connexion, sparsely chosen.

- In usual PGD formulations, imposing complex boundary conditions become sometimes a tricky issue. The weak (natural) or strong (essential) enforcement of boundary conditions needs performing a separated representation of them, before introducing the former into the weak form and the last in the solution separated representation. However, the formulation just described enables the enforcement of any boundary condition in the most standard way, because only the solution procedure involves the construction of the separated representation of the discrete solution. To prove it, Fig. 2 compares the solution when enforcing a nodal displacement on a point of the boundary of a rectangular domain when using both, the standard finite element

Fig. 2 Comparing FEM and NI-PGD solutions when addressing the enforcement of Dirichlet boundary conditions
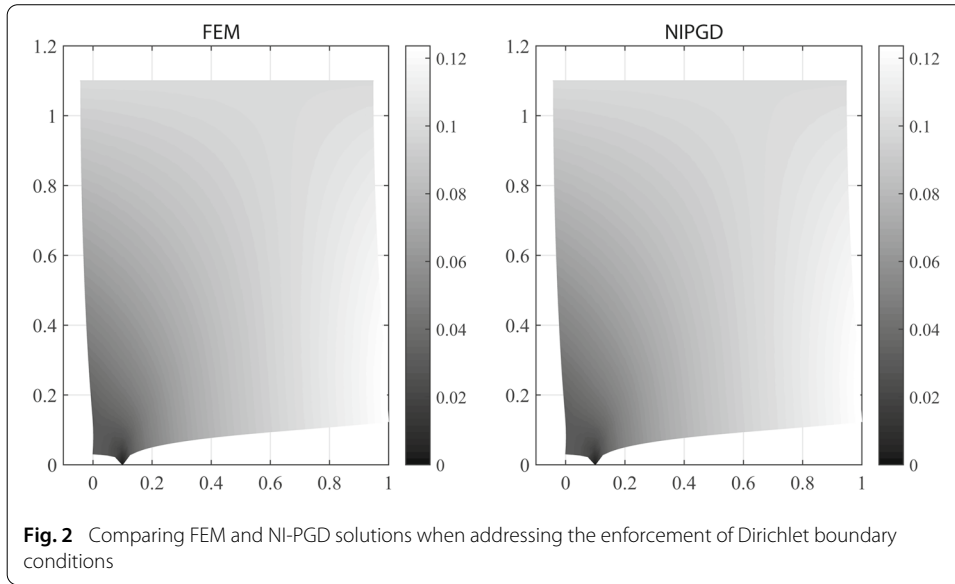
methods and the non-intrusive PGD solver just described. As it can be seen, both solutions agree in minute.

Non-intrusive parametric solver

To circumvent the intrusivity of standard PGD algorithms when considering parameters as extra-coordinates (see [3,4]) enabling the construction of parametric solutions by using commercial simulation softwares, we will consider the simple collocation strategy operating on a hierarchical approximation basis using sparse grids proposed in [27] an summarized below.

We consider the general case in which a transient parametric solution is searched. For the sake of notational simplicity, we assume that only one parameter is involved in the model, $\mu \in [\mu_{min}, \mu_{max}]$. The generalization to several, potentially many parameters is straightforward. The parametric solution $u(\mathbf{x}, \mu)$ is searched in the separated form

$$u(\mathbf{x}, \mu) \approx \sum_{i=1}^{M} X_i(\mathbf{x}) M_i(\mu),$$

where both functions involved in the finite sum representation, $X_i(\mathbf{x})$ and $M_i(\mu)$, are a priori unknown.

Sparse Subspace Learning—SSL—consists first in choosing a hierarchical basis of the parametric domain. The associated collocation points (the Gauss-Lobatto-Chebyshev) and the associated functions will be noted by: $(\mu_i^j, \xi_i^j(\mu))$, where indexes i and j refer to the i-point at the j-level.

At the first level, $j = 0$, there are only to points, μ_1^0 and μ_2^0, that correspond to the minimum and maximum value of the parameters that define the parametric domain, i.e. $\mu_1^0 = \mu_{min}$ and $\mu_2^0 = \mu_{max}$ ($\Omega_\mu = [\mu_{min}, \mu_{max}]$). If we assume that a direct solver is available, i.e., the one separating the nodal unknowns proposed, described and discussed in the previous section, these solutions read

$$u_1^0(\mathbf{x}) = u(\mathbf{x}; \mu = \mu_1^0),$$

and

$$u_2^0(\mathbf{x}) = u(\mathbf{x}; \mu = \mu_2^0),$$

respectively.

Thus, the solution at level $j = 0$ could be approximated from

$$u^0(\mathbf{x}, \mu) = u_1^0(\mathbf{x})\xi_1^0(\mu) + u_2^0(\mathbf{x})\xi_2^0(\mu),$$

that in fact consists of a standard linear approximation since at the first level, $j = 0$, the two approximation functions read

$$\xi_1^0(\mu) = 1 - \frac{\mu - \mu_1^0}{\mu_2^0 - \mu_1^0},$$

and

$$\xi_1^0(\mu) = \frac{\mu - \mu_1^0}{\mu_2^0 - \mu_1^0},$$

respectively.

At level $j = 1$ there is only one point located just in the middle of the parametric domain, i.e. $\mu_1^1 = 0.5 \, (\mu_{min} + \mu_{max})$, being its associated interpolation function $\xi_1^1(\mu)$. It defines a parabola that takes a unit value at $\mu = \mu_1^1$ and vanishes at the other collocation points of level $j = 0$, μ_1^0 and μ_2^0 in this case. The associated solution reads

$$u_1^1(\mathbf{x}) = u(\mathbf{x}; \mu = \mu_1^1).$$

This solution contains a part already explained by the just computed approximation at the previous level, $j = 0$, expressed by

$$u^0(\mathbf{x}, \mu_1^1) = u_1^0(\mathbf{x})\xi_1^0(\mu_1^1) + u_2^0(\mathbf{x})\xi_2^0(\mu_1^1).$$

Thus, we can define the so-called surplus as

$$\tilde{u}_1^1(\mathbf{x}) = u_1^1(\mathbf{x}) - u^0(\mathbf{x}, \mu_1^1),$$

from which the approximation at level $j = 1$ reads

$$u^1(\mathbf{x}, t, \mu) = u^0(\mathbf{x}, \mu) + \tilde{u}_1^1(\mathbf{x})\xi_1^1(\mu). \tag{22}$$

The process continues by adding surpluses when going-up with the hierarchical approximation level. An important aspect is that the norm of the surplus can be used as a local error indicator, and then when adding a level does not contribute sufficiently, the sampling process can stop.

The computed solution, as noticed in Eq. (22), ensures a separated representation. However, it could contain too many terms. In that circumstances a post-compression takes place by looking for a more compact separated representation, as previously discussed and addressed in [4].

When the model involves more parameters, e.g., μ and η, the hierarchical 2D basis, defined in the parametric space (μ, η) is composed by the cartesian product of the collocations points and the tensor product of the approximation bases $\xi_i^0(\mu)$ and $\varphi_j^0(\eta)$.

Thus, the first level $j = 0$, is composed by the four points:

$$(\mu_1^0, \eta_1^0), \ (\mu_2^0, \eta_1^0), \ (\mu_2^0, \eta_2^0), \ (\mu_1^0, \eta_2^0),$$

with the associated interpolation functions

$$\xi_1^0(\mu)\varphi_1^0(\varphi), \ \xi_2^0(\mu)\varphi_1^0(\eta), \ \xi_2^0(\mu)\varphi_2^0(\eta), \ \xi_1^0(\mu)\varphi_2^0(\eta).$$

When moving to the next level, $j = 1$, the collocation points and approximation functions result from the combination of the zero-level of one parameter and the first level of the second one, i.e., the points are now: $(\mu_1^0, \eta_1^1), \ (\mu_2^0, \eta_1^1)$ and $(\mu_1^1, \eta_1^0), \ (\mu_1^1, \eta_2^0)$. In what concerns the interpolation functions they result from the product of the zero level in one coordinate and the level one in the other. It is worth noting that the point (μ_1^1, η_1^1) and its associated interpolation function is in fact a term of level $j = 2$.

As it can be noticed, the procedure only needs the calculation of the solution for some values of the parameters. This solution can be performed by using any available software. It is in that sense that the procedure is qualified as non-intrusive.

Numerical results

In this section, and in order to prove the potentialities of both non-intrusive procedures just described, the one related to the space separation and the other to the parametric solutions, we address elastic homogenization on the representative domain associated with the 3D woven fabric depicted in Fig. 1.

Concerning the homogenization, 2D/1D decompositions will be considered to check the compactness of the computed solutions, that is, the number of terms involved in both finite sum decompositions.

Concerning the parametric study damage envelopes with respect to the deformation (related to a planar stress assumption) applied on the representative domain will be obtained by using the superposition principle, whose validity is guaranteed by the linearity of the assumed elastic behavior.

Finally, parametric solutions will be considered for performing a sensitivity analysis of homogenized properties with respect to the microscopic features.

Elastic homogenization

The so-called layer to layer 3D woven fabric, constituted by warps, wefts and blinder yarns, depicted in Fig. 3 is considered here, and was previously addressed in [28–30].

The mesh used in this study is based on a voxel representation. The yarn mechanical properties are obtained by using the Mori-Tanaka model, by considering the fibres and matrix mechanical properties reported in Table 1.

The microstructural geometric complexity as well as the fact that the microscopic mechanical properties evolve all along the representative cell because the phase fluctuations induced by the forming process itself, make difficult a microstructural separated representation, supporting the choice of performing a standard discretization of the elastic problem in the representative cell, with the adequate boundary conditions ensuring the
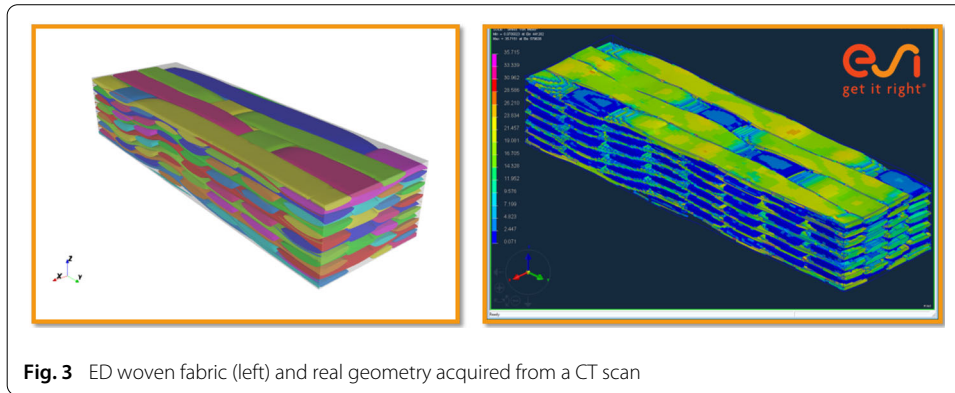
Fig. 3 ED woven fabric (left) and real geometry acquired from a CT scan

Table 1 Fibre and matrix mechanical properties considered to derive the yarn homogeni zed properties

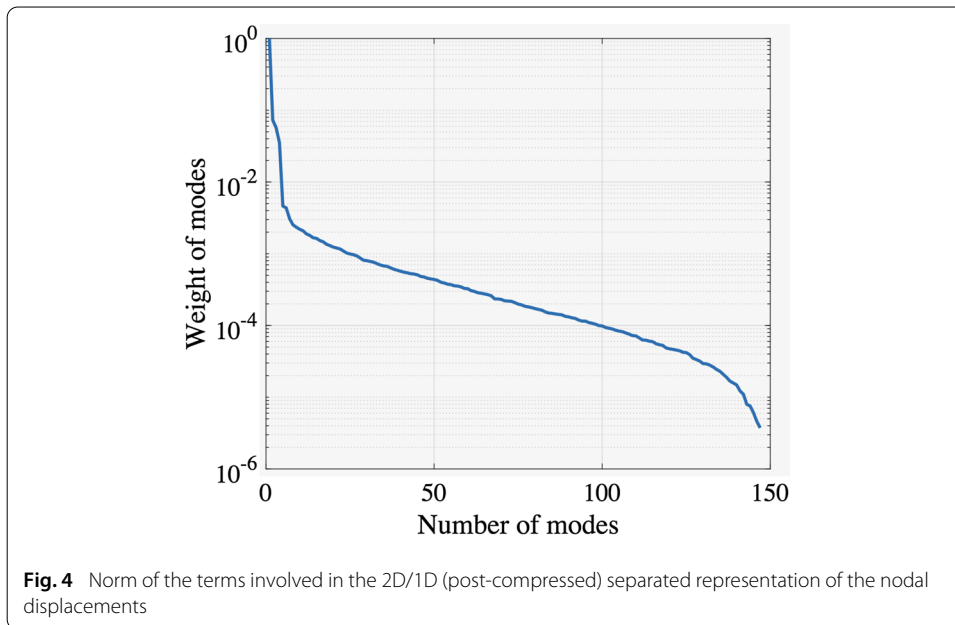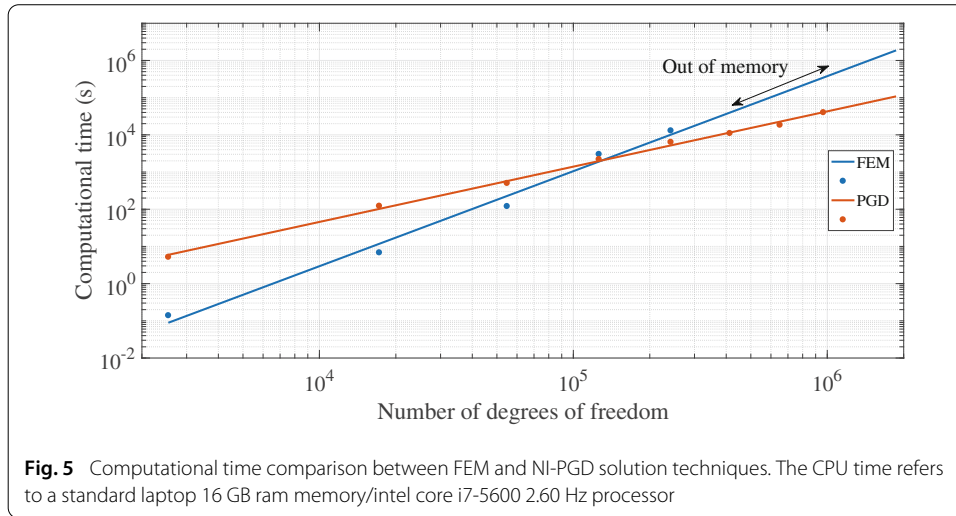|	E_{11}	E_{22}	E_{33}	G_{12}	G_{23}	G_{13}	v_{12}	v_{23}	v_{13}
Fiber	261.055	16.1332	16.1332	13.6837	10	10	0.289	0.3	0.3
Matrix	2.89	2.89	2.89	1.11	1.11	1.11	0.3	0.3	0.3

Fig. 4 Norm of the terms involved in the 2D/1D (post-compressed) separated representation of the nodal displacements

fulfillment of the so-called Hill-Mandel conditions [31, 32], and then applied a separated representation to the vector containing the unknown nodal displacements.

Extraction of effective properties

Figure 4 represents the norm of the different terms of the finite sum, from which it can be noticed that the firsts are the most important for describing the solution, whereas the ones related to smaller norm are describing the microscopic features of the solution.Appropriate error estimators [33, 34] should be considered for stopping the enrichment process and then truncating the separated representation to a finite sum as reduced as possible with respect to the desired accuracy.

Fig. 5 Computational time comparison between FEM and NI-PGD solution techniques. The CPU time refers to a standard laptop 16 GB ram memory/intel core i7-5600 2.60 Hz processor

The homogenized properties were in perfect agreement to the ones derived with a standard procedure. The main interest of using the separated representation was the fact of reaching very fine levels of resolution while speeding-up the solution with respect to procedures based on direct or iterative solvers of the resulting linear system. Figure 5 compares the computing time related to the use of a standard linear system solution with the one associated to the separated constructor (NI-PGD), proving the superiority of the last when the system size increases.

Initial damage envelopes

Initial damage envelopes were considered for analyzing pre-impregnated composite configurations. In the present 3D case, they describe the combination of effective deformations on the representative domain leading to damage initiation. Because the intense anisotropy the combination of strains leading to damage results in complex surfaces (in the strain space) where points in the interior experience elastic behaviour whereas points on the surface represents loadings leading to damage initiation.

The generation of those surfaces separating undamaged and damaged regions requires solving the elastic problem for a variety of loadings (strains) and identifying the ones that activate one of the damage modes (related to fibres or matrix). In general failure starts with the matrix damage and progresses with transverse yarn damage towards the final fibre failure.

We consider a mesh on the strain space composed of 600,000 points representing different combination of the different strain components. Then each one was affected by a scalar (strain intensity) that was increased until the first failure mode occurs. This point represent a point on the failure surface.

In order to alleviate the computational cost, and being, until failure, the problem linear, one could take advantage of the superposition principle, and therefore, solving the elastic problem in the representative domain, for each component of the strain taking a unit value, vanishing all the others. Any possible combination is the obtained by superposing the unitary solutions affected by the scalar intensity factor. These envelopes can be obtained very efficiently for any failure mode in order to compare them.

Table 2 Damage model for yarns and matrix

Fibre failure	Initial transverse damage under compression inside yarns
$f_{ft} = \dfrac{\epsilon_a}{\epsilon_t} = 1$	$f_{mat} = \left(\dfrac{\tau_T}{S_T - \mu_T \sigma_n}\right)^2 + \left(\dfrac{\tau_L}{S_L - \mu_L \sigma_n}\right)^2 = 1$
Initial matrix damage	**Initial transverse damage under tension inside yarns**
$\Phi_m^d = \dfrac{3J_2}{X_m^c X_m^t} + \dfrac{I_1 \left(X_m^c - X_m^t\right)}{X_m^c X_m^t}$	$f_{mat} = \left(\dfrac{\sigma_n}{Y_T}\right)^2 + \left(\dfrac{\tau_T}{S_T}\right)^2 + \left(\dfrac{\tau_L}{S_L}\right)^2 = 1$

Table 3 Parameters involved in the failure models

E_T	E_C	Y_T (GPa)	Y_C (GPa)	S_L (GPa)	X_t (GPa)	X_c (GPa)
0.018	0.018	70	200	100	93	124
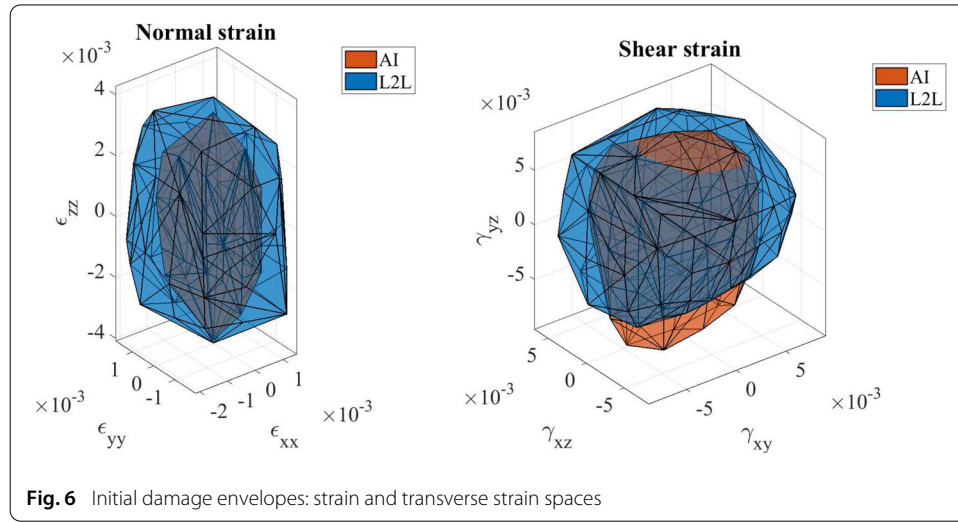
Fig. 6 Initial damage envelopes: strain and transverse strain spaces

In our numerical results we assumed the damage model reported in [35,36] and summarized in Table 2, where I_1 and J_2 are the first and second invariant of the effective stress tensor; σ_n, σ_T and σ_L are the failure tensions normal, transverse and longitudinal respectively to the crack plane, with the other parameters given in Table 3.

Figure 6 shows the initial damage envelope for the representative cell for both, normal and shear strain and for two different 3D woven fabric configuration, layer to layer and angle interlock Fig. 7.

Sensitivity analysis

In the present case and using the non-intrusive parametric solution procedure, we considered the homogenization problem but now by adding as extra-coordinates the material parametres E_m, E_{11}, E_{22}, G_{12}. Once the parametric space is created, the homogenized properties becomes parametric with respect to the phases properties, making possible to evaluate in real-time the homogenized properties for different values of yarn and matrix elasticity properties. Figure 8 provides a view of the GUI application whose sliders enable choosing the fibre and matrix properties.

One application of this parametric solution is the study of sensibility of macro with respect to the micro-properties. Thus, it is possible to evaluate in real-time the output
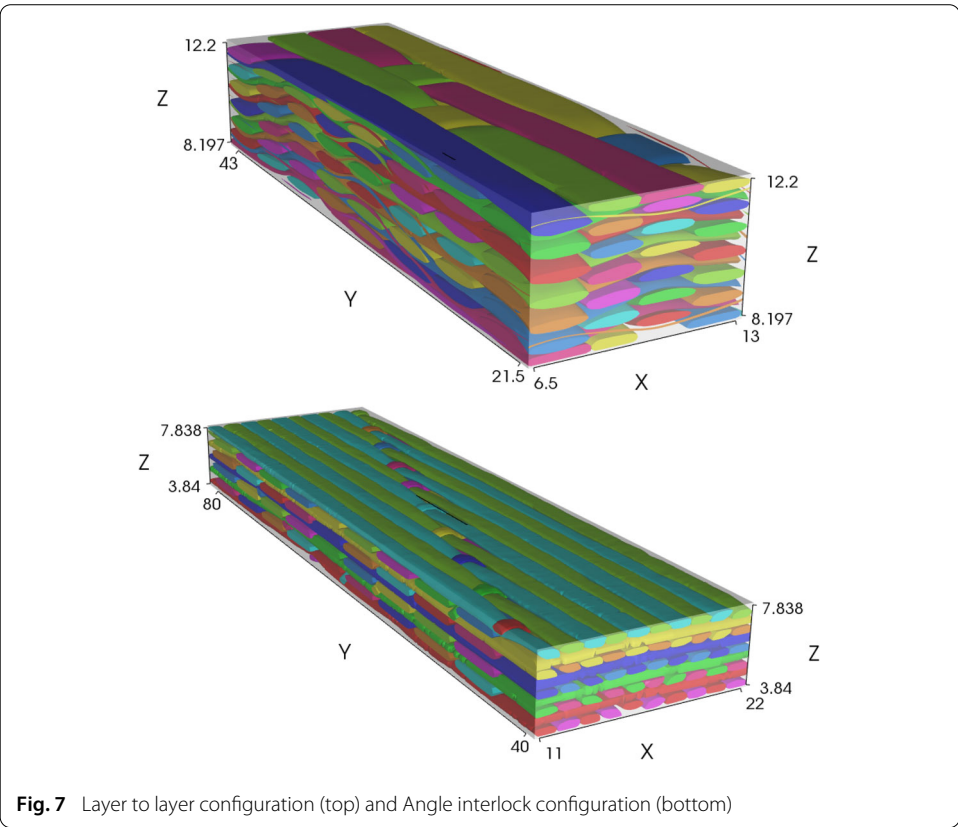
Fig. 7 Layer to layer configuration (top) and Angle interlock configuration (bottom)
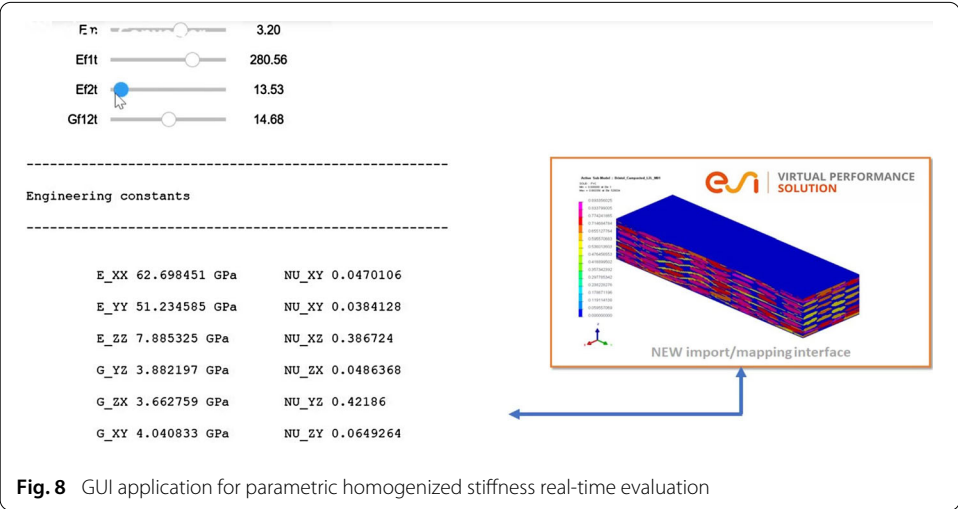

Fig. 8 GUI application for parametric homogenized stiffness real-time evaluation

variation (in %) with respect to a given variation (in %) of a given input. Table 4 reports these evolutions when enforcing 30% of variation of each input.

Table 4 allows extracting the more relevant parameters with higher impact on the homogenized properties.

Conclusions

In this present work, a non intrusive formulation of PGD is presented. Both space separation and parametric solutions were implemented. Both formulations were successfully

Table 4 Sensitivity analysis

Hom-tensor	E_{11} (%)	E_{22} (%)	E_{33} (%)	G_{12} (%)	G_{13} (%)	G_{23} (%)
Matrix (30 E_m)	7.5	7.5	0.2	0.18	0.18	0.6
Yarn (30 E_{11})	8	12	52	62	64	60

applied for efficiently address homogenization, failure analysis and sensitivity evaluation of complex 3D microstructures as the ones encountered in 3D woven fabrics. The use of the proposed techniques allowed important CPU time savings without affecting the solution accuracy, as well as to explore parametric solutions in almost real-time.

Authors' contributions
All the authors participated in the definition of techniques and algorithms. All authos read and approved the final manuscript.

Author details
[1]ESI Group, Parc Icade, Immeuble le Seville, 3 bis, Saarinen, CP 50229, 94528 Rungis Cedex, France, [2]ESI Group chair @ PIMM, Arts et Metiers Institute of Technology, 151 Boulevard de l'Hopital, 75013 Paris, France.

Competing interests
The authors declare that they have no competing interests.

Appendix A: Revisiting the in-plane-out-of-plane separated representation constructor

We consider the model related to the steady state heat conduction equation:

$$\nabla \cdot (\mathbf{K}\nabla u) = 0, \tag{23}$$

in a plate geometry that contains P plies composing the plate thickness. Each ply is characterized by given conductivity tensor $\mathbf{K}_i(x, y) \equiv \mathbf{K}_i(\mathbf{x})$ which is assumed constant through the ply thickness. Moreover, without any loss of generality, we assume the same thickness h ($h = H/P$) for the different layers of the laminate. Thus, we can define a characteristic function representing the position of each layer $i = 1, \ldots, P$:

$$\chi_i(z) = \begin{cases} 1, & z_i \leq z \leq z_{i+1} \\ 0, & \text{otherwise} \end{cases}, \tag{24}$$

where $z_i = (i - 1)h$ defines the location of ply i in the laminate thickness. Now, the laminate conductivity can be given in the following separated form:

$$\mathbf{K}(x, y, z) = \sum_{i=1}^{i=P} \mathcal{K}_i(\mathbf{x})\chi_i(z), \tag{25}$$

with $\mathcal{K}_i$ the conductivity tensor of the i-ply.

The weak form of Eq. (23), when assuming Dirichlet boundary conditions, writes:

$$\int_{\Xi} \nabla u^* \cdot (\mathbf{K} \nabla u) \ d\Xi = 0, \tag{26}$$

with the test function u^* defined in an appropriate functional space. The solution $u(x, y, z)$ is searched under the separated form:

$$u(\mathbf{x}, z) \approx \sum_{j=1}^{N} X_j(\mathbf{x}) \cdot Z_j(z). \tag{27}$$

In what follows we are illustrating the construction of such a decomposition. For this purpose we assume that at enrichment step $n < N$ the solution $u^n(\mathbf{x}, z)$ is already known:

$$u^n(\mathbf{x}, z) = \sum_{j=1}^{n} X_j(\mathbf{x}) \cdot Z_j(z), \tag{28}$$

and that at the present step $n + 1$ we look for the solution enrichment $R(\mathbf{x}) \cdot S(z)$:

$$u^{n+1}(\mathbf{x}, z) = u^n(\mathbf{x}, z) + R(\mathbf{x}) \cdot S(z). \tag{29}$$

The test function involved in the weak form is searched under the form:

$$u^*(\mathbf{x}, z) = R^*(\mathbf{x}) \cdot S(z) + R(\mathbf{x}) \cdot S^*(z). \tag{30}$$

By introducing Eqs. (29) and (30) into Eq. (26) it results:

$$\int_{\Xi} \left(\begin{pmatrix} \tilde{\nabla} R^* \cdot S \\ R^* \cdot \frac{dS}{dz} \end{pmatrix} + \begin{pmatrix} \tilde{\nabla} R \cdot S^* \\ R \cdot \frac{dS^*}{dz} \end{pmatrix} \right) \cdot \left(\mathbf{K} \begin{pmatrix} \tilde{\nabla} R \cdot S \\ R \cdot \frac{dS}{dz} \end{pmatrix} \right) \ d\Xi$$
$$= -\int_{\Xi} \left(\begin{pmatrix} \tilde{\nabla} R^* \cdot S \\ R^* \cdot \frac{dS}{dz} \end{pmatrix} + \begin{pmatrix} \tilde{\nabla} R \cdot S^* \\ R \cdot \frac{dS^*}{dz} \end{pmatrix} \right) \cdot \mathbf{Q}^n \ d\Xi, \tag{31}$$

where $\tilde{\nabla}$ denotes the plane component of the gradient operator, i.e. $\tilde{\nabla} = \left(\frac{\partial}{\partial x}, \frac{\partial}{\partial y} \right)^T$ and $\mathbf{Q}^n$ denotes the flux at iteration n:

$$\mathbf{Q}^n = \mathbf{K} \sum_{j=1}^{n} \begin{pmatrix} \tilde{\nabla} X_j(\mathbf{x}) \cdot Z_j(z) \\ X_j(\mathbf{x}) \cdot \frac{dZ_j(z)}{dz} \end{pmatrix}. \tag{32}$$

Now, as the enrichment process is nonlinear we propose to search the couple of functions $R(\mathbf{x})$ and $S(z)$ by applying the alternate direction fixed point algorithm. Thus, assuming $R(\mathbf{x})$ known, we compute $S(z)$, and then we update $R(\mathbf{x})$. The process continues until reaching convergence. The converged solutions allow defining the next term in the finite sum decomposition, i.e. $R(\mathbf{x}) \rightarrow X_{n+1}(\mathbf{x})$ and $S(z) \rightarrow Z_{n+1}(z)$.

We are illustrating each one of the just referred steps.

A.1 Computing $R(\mathbf{x})$ from $S(z)$

When $S(z)$ is known the test function reduces to:

$$u^*(\mathbf{x}, z) = R^*(\mathbf{x}) \cdot S(z), \tag{33}$$

and the weak form (31) reduces to:

$$\int_\Xi \begin{pmatrix} \tilde{\nabla} R^* \cdot S \\ R^* \cdot \frac{dS}{dz} \end{pmatrix} \cdot \left(\mathbf{K} \begin{pmatrix} \tilde{\nabla} R \cdot S \\ R \cdot \frac{dS}{dz} \end{pmatrix} \right) d\Xi = -\int_\Xi \begin{pmatrix} \tilde{\nabla} R^* \cdot S \\ R^* \cdot \frac{dS}{dz} \end{pmatrix} \cdot \mathbf{Q}^n \, d\Xi. \tag{34}$$

Now, as all the functions involving the coordinate z are known, they can be integrated over $\mathcal{I} = [0, H]$. Thus, if we consider:

$$\mathbf{K} = \begin{pmatrix} \mathbb{K} & \mathbf{k} \\ \mathbf{k}^T & \kappa \end{pmatrix}, \tag{35}$$

with

$$\mathbb{K} = \begin{pmatrix} \mathbf{K}_{xx} & \mathbf{K}_{xy} \\ \mathbf{K}_{xy} & \mathbf{K}_{yy} \end{pmatrix}, \tag{36}$$

$$\mathbf{k} = \begin{pmatrix} \mathbf{K}_{xz} \\ \mathbf{K}_{yz} \end{pmatrix} \tag{37}$$

and $\kappa = \mathbf{K}_{zz}$, then we can define:

$$\mathbf{K}^x = \begin{pmatrix} \int_\mathcal{I} \mathbb{K} \cdot S^2 \, dz & \int_\mathcal{I} \mathbf{k} \cdot \frac{dS}{dz} \cdot S \, dz \\ \int_\mathcal{I} \mathbf{k}^T \cdot \frac{dS}{dz} \cdot S \, dz & \int_\mathcal{I} \kappa \cdot \left(\frac{dS}{dz} \right)^2 dz \end{pmatrix} \tag{38}$$

and

$$(\mathbf{Q}^x)^n = \sum_{j=1}^{j=n} \left(\begin{pmatrix} \int_\mathcal{I} \mathbb{K} \cdot S \cdot Z_j \, dz & \int_\mathcal{I} \mathbf{k} \cdot \frac{dZ_j}{dz} \cdot S \, dz \\ \int_\mathcal{I} \mathbf{k}^T \cdot \frac{dS}{dz} \cdot Z_j \, dz & \int_\mathcal{I} \kappa \cdot \frac{dS}{dz} \cdot \frac{dZ_j}{dz} \, dz \end{pmatrix} \cdot \begin{pmatrix} \tilde{\nabla} X_j(\mathbf{x}) \\ X_j(\mathbf{x}) \end{pmatrix} \right) \tag{39}$$

that allows writing Eq. (34) into the form:

$$\int_\Omega \begin{pmatrix} \tilde{\nabla} R^* \\ R^* \end{pmatrix} \cdot \left(\mathbf{K}^x \begin{pmatrix} \tilde{\nabla} R \\ R \end{pmatrix} \right) d\Omega = -\int_\Omega \begin{pmatrix} \tilde{\nabla} R^* \\ R^* \end{pmatrix} \cdot (\mathbf{Q}^x)^n \, d\Omega, \tag{40}$$

that defines an elliptic 2D problem in Ω.

A.2 Computing $S(z)$ from $R(\mathbf{x})$

When $R(\mathbf{x})$ is known the test function writes:

$$p^*(\mathbf{x}, z) = R(\mathbf{x}) \cdot S^*(z) \tag{41}$$

and the weak form (31) reduces to:

$$\int_\Xi \begin{pmatrix} \tilde{\nabla} R \cdot S^* \\ R \cdot \frac{dS^*}{dz} \end{pmatrix} \cdot \left(\mathbf{K} \begin{pmatrix} \tilde{\nabla} R \cdot S \\ R \cdot \frac{dS}{dz} \end{pmatrix} \right) d\Xi = -\int_\Xi \begin{pmatrix} \tilde{\nabla} R \cdot S^* \\ R \cdot \frac{dS^*}{dz} \end{pmatrix} \cdot \mathbf{Q}^n \, d\Xi. \tag{42}$$

Now, as all the functions involving the in-plane coordinates $\mathbf{x} = (x, y)$ are known, they can be integrated over Ω. Thus, using the previous notation we can define:

$$\mathbf{K}^z = \begin{pmatrix} \int_\Omega (\tilde{\nabla} R) \cdot (\mathbb{K} \cdot \tilde{\nabla} R) \, d\Omega & \int_\Omega (\tilde{\nabla} R) \cdot \mathbf{k} \cdot R \, d\Omega \\ \int_\Omega (\tilde{\nabla} R) \cdot \mathbf{k} \cdot R \, d\Omega & \int_\Omega \kappa \cdot R^2 \, d\Omega \end{pmatrix}, \tag{43}$$

and

$$(\mathbf{Q}^z)^n = \sum_{j=1}^{j=n} \left(\begin{pmatrix} \int_\Omega (\tilde{\nabla} R) \cdot (\mathbb{K} \cdot \tilde{\nabla} X_j) \, d\Omega & \int_\Omega (\tilde{\nabla} R) \cdot \mathbf{k} \cdot X_j \, d\Omega \\ \int_\Omega (\tilde{\nabla} X_j) \cdot \mathbf{k} \cdot R \, d\Omega & \int_\Omega \kappa \cdot X_j \cdot R \, d\Omega \end{pmatrix} \cdot \begin{pmatrix} Z_j(z) \\ \frac{dZ_j}{dz}(z) \end{pmatrix} \right), \tag{44}$$

that allows writing Eq. (42) into the form:

$$\int_\mathcal{I} \begin{pmatrix} S^* \\ \frac{dS^*}{dz} \end{pmatrix} \cdot \left(\mathbf{K}^z \begin{pmatrix} S \\ \frac{dS}{dz} \end{pmatrix} \right) \, dz = - \int_\mathcal{I} \begin{pmatrix} S^* \\ \frac{dS^*}{dz} \end{pmatrix} \cdot (\mathbf{Q}^z)^n \, dz \tag{45}$$

that defines a one-dimensional boundary value problem (BVP).

References

1. Ammar A, Mokdad B, Chinesta F, Keunings R. A new family of solvers for some classes of multidimensional partial differential equations encountered in kinetic theory modeling of complex fluids. J Non-Newton Fluid Mech. 2006;139:153–76.
2. Chinesta F, Ladeveze P, Cueto E. A short review in model order reduction based on proper generalized decomposition. Arch Comput Methods Eng. 2011;18:395–404.
3. Chinesta F, Leygue A, Bordeu F, Aguado JV, Cueto E, Gonzalez D, Alfaro I, Ammar A, Huerta A. Parametric PGD based computational vademecum for efficient design, optimization and control. Arch Comput Methods Eng. 2013;20(1):31–59.
4. Chinesta F, Keunings R, Leygue A. The proper generalized decomposition for advanced numerical simulations. A primer. New York: Springer; 2013.
5. Leon A, Barasinski A, Abisset E, Cueto E, Chinesta F. Wavelet-based multiscale proper generalized decomposition. Comptes Rendus Mecanique. 2018;346:485–500.
6. Bognet B, Leygue A, Chinesta F, Poitou A, Bordeu F. Advanced simulation of models defined in plate geometries: 3D solutions with 2D computational complexity. Comput Methods Appl Mech Eng. 2012;201:1–12.
7. Bognet B, Leygue A, Chinesta F. Separated representations of 3D elastic solutions in shell geometries. Adv Model Simul Eng Sci. 2014;1:4.
8. Leygue A, Chinesta F, Beringhier M, Nguyen TL, Grandidier JC, Pasavento F, Schrefler B. Towards a framework for non-linear thermal models in shell domains. Int J Num Methods Heat Fluid Flow. 2013;23(1):55–73.
9. Bordeu F, Ghnatios Ch, Boulze D, Carles B, Sireude D, Leygue A, Chinesta F. Parametric 3D elastic solutions of beams involved in frame structures. Adv Aircr Spacecr Sci. 2015;2(3):233–48.
10. Gallimard L, Vidal P, Polit O. Coupling finite element and reliability analysis through proper generalized decomposition model reduction. Int J Num Methods Eng. 2013;95(13):1079–93.
11. Vidal P, Gallimard L, Polit O. Composite beam finite element based on the proper generalized decomposition. Comput Struct. 2012;102:76–86.
12. Vidal P, Gallimard L, Polit O. Proper generalized decomposition and layer-wise approach for the modeling of composite plate structures. Int J Solids Struct. 2013;50(14–15):2239–50.
13. Vidal P, Gallimard L, Polit O. Explicit solutions for the modeling of laminated composite plates with arbitrary stacking sequences Composites Part B -. Engineering. 2014;60:697–706.
14. Vidal P, Gallimard L, Polit O. Shell finite element based on the proper generalized decomposition for the modeling of cylindrical composite structures. Comput Struct. 2014b;132:1–11.
15. Vidal P, Gallimard L, Polit O. Assessment of variable separation for finite element modeling of free edge effect for composite plates. Compos Struct. 2015;123:19–29.
16. Giner E, Bognet B, Rodenas JJ, Leygue A, Fuenmayor J, Chinesta F. The proper generalized decomposition (PGD) as a numerical procedure to solve 3D cracked plates in linear elastic fracture mechanics. Int J Solid Struct. 2013;50(10):1710–20.
17. Metoui S, Pruliere E, Ammar A, Dau F, Iordanoff I. The proper generalized decomposition for the simulation of delamination using cohesive zone model. Int J Num Methods Eng. 2014;99(13):1000–22.
18. Chinesta F, Leygue A, Bognet B, Ghnatios Ch, Poulhaon F, Bordeu F, Barasinski A, Poitou A, Chatel S, Maison-Le-Poec S. First steps towards an advanced simulation of composites manufacturing by automated tape placement. Int J Mater Form. 2014;7(1):81–92.

19. Nazeer M, Bordeu F, Leygue A, Chinesta F. Arlequin based PGD domain decomposition. Comput Mech. 2014;54(5):1175–90.
20. Ammar A, Chinesta F, Cueto E. Coupling finite elements and proper generalized decompositions. Int J Multiscale Comput Eng. 2011;9(1):17–33.
21. Ghnatios Ch, Chinesta F, Binetruy Ch. The squeeze flow of composite laminates. Int J Mater Form. 2015;8:73–83.
22. Chinesta F, Ammar A, Leygue A, Keunings R. An overview of the proper generalized decomposition with applications in computational rheology. J Non Newton Fluid Mech. 2011;166:578–92.
23. Canales D, Leygue A, Chinesta F, Alfaro I, Gonzalez D, Cueto E, Feulvarch E, Bergheau JM. In-plane-out-of-plane separated representations of updated-Lagrangian descriptions of thermomechanical models defined in plate domains. Comptes Rendus Mécanique. 2016;344:225–35.
24. Dumon A, Allery C, Ammar A. Proper general decomposition (PGD) for the resolution of Navier–Stokes equations. J Comput Phys. 2011;230(4):1387–407.
25. Dumon A, Allery C, Ammar A. Proper Generalized Decomposition method for incompressible Navier–Stokes equations with a spectral discretization. Appl Math Comput. 2013;219(15):8145–62.
26. Dumon A, Allery C, Ammar A. Simulation of heat and mass transport in a square lid-driven cavity with proper generalized decomposition. Num Heat Transf B. 2013b;63(1):18–43.
27. Borzacchiello D, Aguado JV. Non-intrusive sparse subspace learning for parametrized problems. Arch Comput Methods Eng. 2017;. https://doi.org/10.1007/s11831-017-9241-4.
28. Green SD, Matveev MY, Long AC, Ivanov D, Hallet SR. Mechanical modelling of 3D woven composites considering realistic unit cell geometry. Compos Struct. 2014;118:284–93.
29. Green SD, Long AC, El Said BSF, Hallet SR. Numerical modelling of 3D woven preform deformations. Compos Struct. 2014;108:747–56.
30. El Said BSF, Green S. Hallet SR Kinematic modelling of 3D woven fabric deformation for structural scale features. Composites. 2014;57:95–107.
31. Hill R. Elatic properties of reinforced solid: some theoretical principles. J Mech Phys Solids. 1963;11:357–72.
32. Hill R. On constitutive macro-variables for heterogeneous solids at finite strain. Proc R Soc Lond. 1972;326:131–47.
33. Alfaro I, Gonzalez D, Zlotnik S, Diez P, Cueto E. Chinesta F An error estimator for real-time simulators based on model order reduction. Adv Model Simul Eng Sci. 2015;2:30.
34. Chamoin L, Pled F, Allier P, Ladeveze P. A posteriori error estimation and adaptive strategy for PGD model reduction applied to parametrized linear parabolic problems. Comput Methods Appl Mech Eng. 2017;327:118–46.
35. Pinho ST, Lannucci L, Robinson P. Physically-based failure models and criteria for laminate fibre-reinforced composites with emphasis on fibre kinking. Composites. 2006;37:63–73.
36. Melro AR, Camanho PP, Andrade Pires FM. Pinho ST Micromechanical analysis of polymer composites reinforced by unidirectional fibres: Part I Consisting modelling. Int J Solids Struc. 2013;50:1906–15.